IOP Publishing New J. Phys. 27 (2025) 064104 https://doi.org/10.1088/1367-2630/adde7f

New Journal of Physics
The open access journal at the forefront of physics

Deutsche Physikalische Gesellschaft DPG
IOP Institute of Physics

Published in partnership with: Deutsche Physikalische Gesellschaft and the Institute of Physics

OPEN ACCESS

RECEIVED
7 February 2025

REVISED
16 May 2025

ACCEPTED FOR PUBLICATION
29 May 2025

PUBLISHED
6 June 2025

PAPER

Feedback-assisted quantum nondemolition measurement in an atom-light-correlated interferometer

Gao-Feng Jiao

School of Semiconductor and Physics, North University of China, Taiyuan 030051, People's Republic of China

E-mail: gfjiao@foxmail.com

Keywords: quantum measurement, interferometer, quantum correlation

Abstract

Quantum nondemolition (QND) measurement plays an essential role in quantum optics and quantum information. Here, a feedback-assisted atom-light-correlated interferometer (FALCI) is proposed and applied to the QND measurement of photon number, in which the phase of the probe acquires information about the photon number of the signal without perturbing it due to the AC-Stark effect. A beam splitter with adjustable reflectivity is employed as a feedback controller to enhance the performance of QND measurement. The FALCI harnesses interference between quantum-correlated atoms and light to perform the measurement. It is found that the quantum correlation can be enhanced by manipulating the feedback ratio. Furthermore, the QND measurement sensitivity is theoretically studied via homodyne detection. It is demonstrated that the FALCI can achieve the sensitivity enhancement with suitable feedback ratio. For the lossy case, feedback control can mitigate the effect of losses on the sensitivity.

1. Introduction

Quantum nondemolition (QND) measurement is an important tool for engineering and manipulating quantum systems in the field of quantum precision measurement [1–5]. In a QND measurement, a signal is coupled to a probe through an interaction, such that the information about the signal can be obtained indirectly by performing the measurement on the probe. The key to achieving QND measurement is conceiving the measurement scheme in which the back action noise brought by the measurement is transferred to the conjugate observable that we are not concerned about, that is, the probe reveals information about the signal without causing further perturbation to it. The QND measurement has been implemented successfully in various precision measurement applications, such as squeezed state preparation [6–8] and gravitational wave detection [9, 10].

Accurate measurement of photon number is a cornerstone in quantum optics, enabling precise control and detection of quantum states in various applications, including quantum computing [11], quantum information [12], and fundamental physics research [6]. In the quantum optics community, the usual approach to QND measurement of photon number is encoding the photon number of a signal into the phase shift of a probe through a cross-Kerr interaction [13–19]. The problem of determining photon number is transformed into the problem of determining the phase shift. Nevertheless, the major impediments to QND measurement using the optical Kerr effect are the small value of nonlinearity and the photon absorption. This leads to the small phase shift which is difficult to distinguish and measure. There are two main methods to further enhance the performance of QND measurement. The first one is to improve the nonlinear effect for QND measurement, for example, schemes utilizing cavity or circuit quantum electrodynamical systems have enabled photon number QND measurement through strong coupling between the signal and the probe [20–27]. The second is to exploit the higher precision detection scheme for QND measurement [28–30]. Here we focus on the second method.

More recently, coherent feedback control [31–33] that feeds the output of the controlled system back into the input to evolve the quantum system towards a desired result has resulted in various applications, such as quantum state preparation [34–38], quantum enhanced metrology [39–42] and so on [43, 44]. Inspired by

the employment of coherent feedback control to manipulate quantum systems, in this work we propose a feedback-assisted atom-light-correlated interferometer (FALCI) and apply it to QND measurement of photon number. Compared to the prior works involving atom-light hybrids [28–30], in this paper, we introduce a feedback structure to manipulate the interference between quantum-correlated atoms and light. It is demonstrated that the quantum correlation and the QND measurement sensitivity can be enhanced with suitable feedback ratio. Furthermore, feedback control can mitigate the effect of losses on the QND measurement.

This paper is organized as follows. In section 2, we introduce the theoretical model of the FALCI, and investigate the quantum correlation enhancement with the change of feedback ratio. In section 3, we study the QND measurement sensitivity in both lossless and lossy case, feedback control can enhance the performance of the QND measurement and mitigate the effect of losses on the sensitivity. Finally, we summarize the results in section 4.

2. Feedback-assisted atom-light-correlated interferometer

2.1. Model

The schematic of FALCI is shown in figure 1(a), in which two nonlinear Raman processes, NRP1 and NRP2, are utilized to realize the beam splitting and recombination of the quantum-correlated atomic spin wave and optical wave, and a BS with adjustable reflectivity is employed to construct a controllable feedback structure, which feeds part of output field back into the input port. The corresponding energy levels of the atom are given in figure 1(b). A strong pump field A_{p_1} (A_{p_2}) and a weak seed field $\hat{a}_2$ ($\hat{a}_4$) interact with a Λ-shaped atomic ensemble to generate an amplified optical field $\hat{a}_3$ ($\hat{a}_5$) and a correlated atomic spin wave $\hat{S}_1$ ($\hat{S}_3$) via the NRP1 (NRP2).

The Hamiltonian that describes the dynamics of the NRP is given by [45, 46]

$$\hat{H} = i\hbar\eta A_{\mathrm{p}}\hat{a}^{\dagger}\hat{S}^{\dagger} + H.c., \tag{1}$$

where η is the nonlinear coupling coefficient, A_{p} is amplitude of the pump field, and $\hat{S} \equiv (1/\sqrt{N})\sum_k |g\rangle_k\langle m|$ is the spin wave (atomic collective excitation), with N the number of atoms in the ensemble. The input–output relations of NRP1 and NRP2 derived from the above Hamiltonian equation can be written as

$$\hat{a}_3 = G_1\hat{a}_2 + g_1 e^{i\theta_1}\hat{S}_0^{\dagger},\ \hat{S}_1 = G_1\hat{S}_0 + g_1 e^{i\theta_1}\hat{a}_2^{\dagger}, \tag{2}$$

and

$$\hat{a}_5 = G_2\hat{a}_4 + g_2 e^{i\theta_2}\hat{S}_2^{\dagger},\ \hat{S}_3 = G_2\hat{S}_2 + g_2 e^{i\theta_2}\hat{a}_4^{\dagger}, \tag{3}$$

respectively. Here $e^{i\theta_j} = \eta A_{\mathrm{p}_j}/|\eta A_{\mathrm{p}_j}|$, $G_j = \cosh(|\eta A_{\mathrm{p}_j}|\tau)$ and $g_j = \sinh(|\eta A_{\mathrm{p}_j}|\tau)$ are the gain factors, satisfying $G_j^2 - g_j^2 = 1$ $(j = 1, 2)$. τ denotes the pulse duration of pump field. Here $\hat{S}_2 = \hat{S}_1 e^{i\varphi}$ and $\hat{a}_2 = \hat{a}_1 e^{i\phi}$, where φ denotes the phase difference between the two arms of the interferometer and ϕ represents the phase delay introduced by the feedback path.

A BS with adjustable reflectivity is employed as a feedback controller to construct a feedback structure. The input–output relation of the BS controller can be expressed as

$$\hat{a}_1 = \sqrt{1-R}\hat{a}_0 - \sqrt{R}\hat{a}_3, \hat{a}_4 = \sqrt{R}\hat{a}_0 + \sqrt{1-R}\hat{a}_3, \tag{4}$$

where R is the reflectivity of the BS, and the feedback ratio is determined by it. After the feedback controller, one output field $\hat{a}_4$ serves as the input of the NRP2 while the other output field $\hat{a}_1$ is fed back as the input of the NRP1 through a feedback path.

The full input–output relation of the FALCI has the following form

$$\hat{a}_5 = \mathcal{T}_1\hat{a}_0 + \mathcal{T}_2\hat{S}_0^{\dagger}, \hat{S}_3 = \mathcal{T}_3\hat{S}_0 + \mathcal{T}_4\hat{a}_0^{\dagger}, \tag{5}$$

with

$$\mathcal{T}_1 = \frac{G_1G_2e^{i\phi} + g_1g_2\sqrt{1-R}e^{i(\theta_2-\theta_1+\phi-\varphi)} + G_2\sqrt{R}}{G_1\sqrt{R}e^{i\phi} + 1},$$

$$\mathcal{T}_2 = \frac{G_2g_1\sqrt{1-R}e^{i\theta_1} + g_2\sqrt{R}e^{i(\theta_2-\varphi+\phi)} + G_1g_2e^{i(\theta_2-\varphi)}}{G_1\sqrt{R}e^{i\phi} + 1},$$

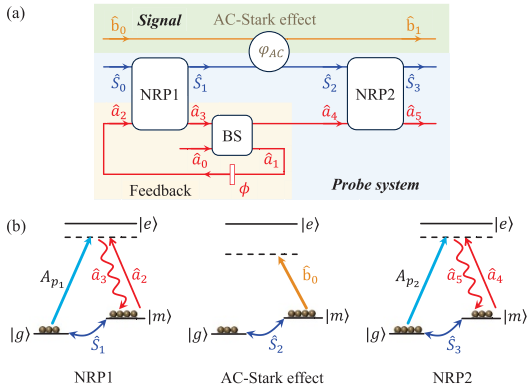

Figure 1. (a) Schematic of QND measurement of photon number. The probe system comprises a feedback-assisted atom-light-correlated interferometer (FALCI), which is achieved utilizing NRP1 and NRP2 as beam splitting and recombination of the quantum-correlated atoms spin wave and optical wave. The feedback scheme is implemented by mixing the output $\hat{a}_3$ of NRP1 and coherent input $\hat{a}_0$ using a BS with adjustable reflectivity. The combined field $\hat{a}_1$ is fed back as the input mode of NRP1 after the phase delay ϕ. (b) Energy levels of the atom. The lower two energy states $|g\rangle$ and $|m\rangle$ are coupled through a higher-energy state $|e\rangle$ by the strong pump field A_{p_1} (A_{p_2}) and the weak seed field $\hat{a}_2$ ($\hat{a}_4$), respectively. $\hat{b}_0$ is far off resonance with the transition $|m\rangle \rightarrow |e\rangle$ by a large detuning. The atomic spin wave $\hat{S}_1$ undergoes a phase shift of φ_{AC} due to the AC-Stark effect by signal light $\hat{b}_0$ and evolves to $\hat{S}_2$. BS, beam splitter; NRP, nonlinear Raman process.

$$\mathcal{T}_3 = \frac{G_1 G_2 e^{i\varphi} + g_1 g_2 \sqrt{1-R} e^{i(\theta_2-\theta_1)} + G_2 \sqrt{R} e^{i(\varphi-\phi)}}{G_1 \sqrt{R} e^{-i\phi} + 1},$$
$$\mathcal{T}_4 = \frac{G_2 g_1 \sqrt{1-R} e^{i(\theta_1+\varphi-\phi)} + g_2 \sqrt{R} e^{i\theta_2} + G_1 g_2 e^{i(\theta_2-\phi)}}{G_1 \sqrt{R} e^{-i\phi} + 1}. \tag{6}$$

2.2. Quantum correlation between atoms and light

Here, we focus on the performance of the quantum correlation between the atomic spin wave and optical wave, which can be characterized by the degree of relative intensity squeezing (DS) defined as the ratio of the quantum fluctuation for the intensity difference between the two output fields to the fluctuation at the standard quantum limit (SQL). Then the DS takes the form of

$$\mathrm{DS} = \frac{\Delta^2\left(\hat{a}_4^\dagger \hat{a}_4 - \hat{S}_1^\dagger \hat{S}_1\right)}{\langle \hat{a}_4^\dagger \hat{a}_4 + \hat{S}_1^\dagger \hat{S}_1 \rangle}, \tag{7}$$

where

$$\Delta^2\left(\hat{a}_4^\dagger \hat{a}_4 - \hat{S}_1^\dagger \hat{S}_1\right) = \left\langle \left(\hat{a}_4^\dagger \hat{a}_4 - \hat{S}_1^\dagger \hat{S}_1\right)^2 \right\rangle - \langle \hat{a}_4^\dagger \hat{a}_4 - \hat{S}_1^\dagger \hat{S}_1 \rangle^2. \tag{8}$$

Without loss of generality, the phase of the NRP1 can be set to zero. The output field $\hat{a}_4$ and $\hat{S}_1$ of the NRP1 under the feedback condition are given by

$$\hat{a}_4 = \mathcal{A}\hat{a}_0 + \mathcal{B}\hat{S}_0^\dagger,\ \hat{S}_1 = \mathcal{C}\hat{S}_0 + \mathcal{D}\hat{a}_0^\dagger, \tag{9}$$

with

$$\mathcal{A} = \frac{G_1 e^{i\phi} + \sqrt{R}}{G_1 \sqrt{R} e^{i\phi} + 1}, \mathcal{B} = \frac{g_1 \sqrt{1-R}}{G_1 \sqrt{R} e^{i\phi} + 1},$$
$$\mathcal{C} = \frac{\sqrt{R} e^{-i\phi} + G_1}{G_1 \sqrt{R} e^{-i\phi} + 1}, \mathcal{D} = \frac{g_1 \sqrt{1-R} e^{-i\phi}}{G_1 \sqrt{R} e^{-i\phi} + 1}. \tag{10}$$

Consider a coherent state together with a vacuum state as input ($\hat{S}_0$ is in a vacuum state). Through equations (7)–(10), one can get the relationship between DS and the feedback ratio R, phase delay ϕ, gain factors G and g as follows

$$\mathrm{DS} = \frac{N_a}{N_a\left(\mathcal{A}\mathcal{A}^* + \mathcal{B}\mathcal{B}^*\right) + 2\mathcal{B}\mathcal{B}^*}, \tag{11}$$

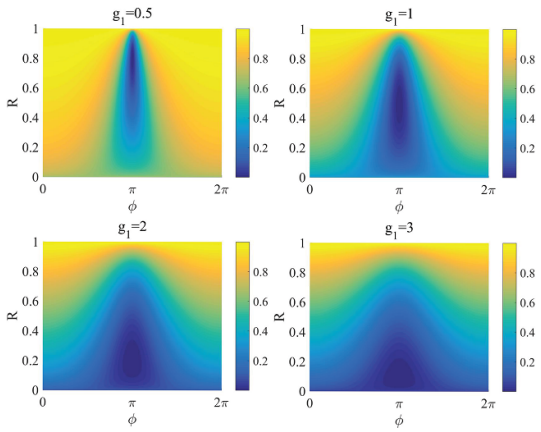

Figure 2. DS as a function of feedback ratio R and phase delay ϕ when $g_1 = 0.5$, $g_1 = 1$, $g_1 = 2$ and $g_1 = 3$, where $N_a = 10$.

where $N_a = \langle \hat{a}_0^\dagger \hat{a}_0 \rangle$. Taking no account of the feedback, i.e. the feedback ratio R and phase delay ϕ are set to zero, the above DS is reduced to

$$\mathrm{DS} = \frac{N_a}{N_a\left(G_1^2 + g_1^2\right) + 2g_1^2}, \tag{12}$$

which is consistent with the result in [47]. Making the bright beam approximation $N_a \gg 1$, the DS becomes $\mathrm{DS} = 1/(2G_1^2 - 1)$. The relative intensity fluctuation $\Delta^2(\hat{a}_4^\dagger \hat{a}_4 - \hat{S}_1^\dagger \hat{S}_1)$ is smaller than SQL by $2G_1^2 - 1$ times, $\hat{a}_4$ and $\hat{S}_1$ is quantum correlated.

Now we analyze the dependence of DS on the feedback ratio R, phase delay ϕ and gain factor g. Figure 2 describes how the feedback ratio R and phase delay ϕ affect the DS when gain factor g_1 is set to 0.5, 1, 2, and 3. As shown in figure 2, when the feedback ratio R and phase ϕ are set within a suitable range, the value of DS is smaller than that of the situation without feedback ($R = 0$), which implies that the quantum correlation between the atomic spin wave and optical wave is enhanced. Nevertheless, note that excessive feedback results in the disappearance of quantum correlation enhancement. That is to say, there exists an optimal feedback ratio that maximizes the quantum correlation. Furthermore, it can be seen that the minimum of DS is obtained when $\phi = \pi$. In this situation, the optimal feedback ratio is found to be $1/G_1^2$. It means that the optimal feedback ratio depends solely on the gain factor, regardless of the input photon number. When the gain factor is known, then the feedback ratio can be manipulated such that the quantum correlation is maximum.

3. QND measurement of photon number

In the previous section, this new type interferometer is introduced in detail, and we can adjust feedback ratio to manipulate and enhance the quantum correlation between the output fields of the interferometer. In this section, it is employed as a probe system for the QND measurement of photon number. The measurement scheme is shown in figure 1. Here, the atom system of the proposed interferometer is subject to the illumination of the signal light $\hat{b}_0$ that is far off resonance with the atomic transition with a large detuning. During the interaction, the phase of the atom probe is shifted by the value depending on the photon number in signal light, can be presented as follows [48, 49]

$$\varphi_{\mathrm{AC}} = \kappa \hat{n}_b, \tag{13}$$

where $\hat{n}_b = \hat{b}_0^\dagger \hat{b}_0$, κ denotes the AC-Stark coefficient, this effect is called AC-Stark effect. The photon number of the signal light is preserved while the phase is perturbed during the interaction, which ensures the fulfillment of the Heisenberg uncertainty principle [50]

$$\Delta n_b \Delta \varphi_b \geqslant 1, \tag{14}$$

Δn_b and $\Delta \varphi_b$ are the uncertainty of photon number and phase for signal light $\hat{b}_0$, respectively. This means that the QND measurement of photon number is accomplished at the cost of increasing the uncertainty in its conjugate observable. By measuring the atomic phase using this interferometer, one can determine the photon number without altering it.

3.1. Sensitivity analysis

Now we analyze the QND measurement sensitivity. The FALCI is studied in a balanced configuration, which corresponds to having $\theta_1 = 0$, $\theta_2 = \pi$ and $g_1 = g_2 = g$, such that with $\varphi = 0$ we have $\mathcal{T}_1 = \mathcal{T}_3 = 1$ and $\mathcal{T}_2 = \mathcal{T}_4 = 0$ and thus $\hat{a}_5 = \hat{a}_0$ and $\hat{S}_3 = \hat{S}_0$ when not considering the feedback (see equation (5)). That is, if there is no phase difference between the two arms of the interferometer, the output fields of the interferometer are equal to the input fields, otherwise, it will lead to a change in the output related to the induced phase shift. In this situation, by setting $\phi = \pi$ for maximum quantum correlation and combining equations (5) and (13), it is found that

$$\hat{a}_5 = \hat{\mathcal{T}}_1\hat{a}_0 + \hat{\mathcal{T}}_2\hat{S}_0^\dagger, \hat{S}_3 = \hat{\mathcal{T}}_3\hat{S}_0 + \hat{\mathcal{T}}_4\hat{a}_0^\dagger, \tag{15}$$

with

$$\begin{aligned}
\hat{\mathcal{T}}_1 &= \frac{g^2\sqrt{1-R}e^{-i\kappa\hat{n}_b} + G\sqrt{R} - G^2}{1 - G\sqrt{R}},\\
\hat{\mathcal{T}}_2 &= \frac{g\sqrt{R}e^{-i\kappa\hat{n}_b} - Gge^{-i\kappa\hat{n}_b} + Gg\sqrt{1-R}}{1 - G\sqrt{R}},\\
\hat{\mathcal{T}}_3 &= \frac{G^2e^{i\kappa\hat{n}_b} - G\sqrt{R}e^{i\kappa\hat{n}_b} - g^2\sqrt{1-R}}{1 - G\sqrt{R}},\\
\hat{\mathcal{T}}_4 &= \frac{-Gg\sqrt{1-R}e^{i\kappa\hat{n}_b} - g\sqrt{R} + Gg}{1 - G\sqrt{R}}.
\end{aligned} \tag{16}$$

Here we consider the homodyne detection of the quadrature $\hat{Y}_{a_5}$, defined as

$$\hat{Y}_{a_5} = -i\left(\hat{a}_5 - \hat{a}_5^\dagger\right). \tag{17}$$

The measurement sensitivity for the photon number in the signal light can be calculated by error propagation formula

$$(\Delta n_b)^2 = \frac{\left(\Delta\hat{Y}_{a_5}\right)^2}{\mathcal{G}^2}, \tag{18}$$

where

$$\mathcal{G} = \frac{\partial\langle\hat{Y}_{a_5}\rangle}{\partial n_b} \tag{19}$$

represents the transfer function,

$$\left(\Delta\hat{Y}_{a_5}\right)^2 = \langle\hat{Y}_{a_5}^2\rangle - \langle\hat{Y}_{a_5}\rangle^2, \tag{20}$$

$\langle\hat{Y}_{a_5}\rangle$ and $\langle\hat{Y}_{a_5}^2\rangle$ are calculated for a given value of n_b, here, for the number state $|n_b\rangle$ of the signal light.

In the case of a coherent state $|\alpha\rangle$ ($\alpha = |\alpha|$) together with a vacuum state $|0\rangle$ as input ($\hat{S}_0$ is in a vacuum state),

$$\begin{aligned}
\mathcal{G} &= -iN_a^{1/2}\partial\left(\mathcal{E} - \mathcal{E}^*\right)/\partial n_b,\\
\left(\Delta\hat{Y}_{a_5}\right)^2 &= \mathcal{E}\mathcal{E}^* + \mathcal{F}\mathcal{F}^*,
\end{aligned} \tag{21}$$

with

$$\begin{aligned}
\mathcal{E} &= \frac{g^2\sqrt{1-R}e^{-i\kappa n_b} + G\sqrt{R} - G^2}{1 - G\sqrt{R}},\\
\mathcal{F} &= \frac{g\sqrt{R}e^{-i\kappa n_b} - Gge^{-i\kappa n_b} + Gg\sqrt{1-R}}{1 - G\sqrt{R}}.
\end{aligned} \tag{22}$$

Clearly, the sensitivity is related to the value of κn_b. In particular, one can verify that the sensitivity achieves its minimum when κn_b is 0 since the transfer function $\mathcal{G}$ and $(\Delta\hat{Y}_{a_5})^2$ respectively sit at their maximum and minimum. The optimal sensitivity is calculated to be

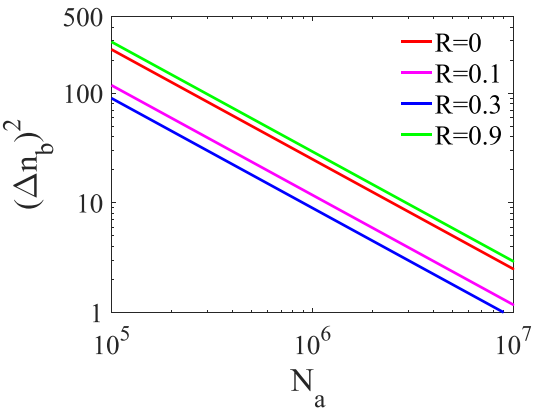

Figure 3. The variation of $(\Delta n_b)^2$ with N_a for different feedback ratio R, where $g = 1$ and $\kappa = 10^{-4}$.

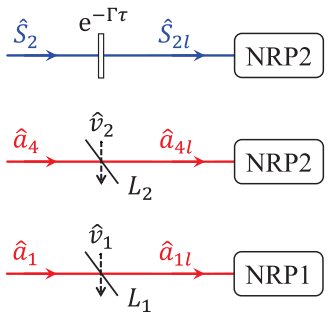

Figure 4. The lossy model. Two virtual beam splitters are introduced to simulate the photon losses. L_j, v_j $(j = 1, 2)$ denote the corresponding reflectivity and introduced vacuum noise. The atomic spin wave $\hat{S}_2$ undergoes collisional dephasing $e^{-\Gamma\tau}$ and becomes $\hat{S}_{2l}$.

$$(\Delta n_b)^2_{\text{opt}} = \frac{\left(g^2\sqrt{1-R} + G\sqrt{R} - G^2\right)^2}{4\kappa^2 N_a g^4 (1-R)} + \frac{\left(g\sqrt{R} - Gg + Gg\sqrt{1-R}\right)^2}{4\kappa^2 N_a g^4 (1-R)}. \tag{23}$$

Figure 3 describes dependence of the optimal sensitivity $(\Delta n_b)^2$ on the input photon number N_a with different feedback ratio, for convenience, we omit the subscript *opt*. The magenta, blue, and green line, respectively, stand for the case that the feedback ratio $R = 0.1$, 0.3 and 0.9. For comparison, the case of $R = 0$ (i.e. no feedback) is also plotted by the red line. It can be observed that the performance of the sensitivity is related to the feedback ratio. In detail, the sensitivity without feedback is worse than that with feedback ratio $R = 0.1$ and 0.3, however, it is better than the case of feedback ratio $R = 0.9$. The result shows that an appropriate feedback ratio can further enhance the sensitivity while the overdone feedback makes the sensitivity worse, which agrees with that obtained by analyzing the dependence of the quantum correlation on the feedback ratio. It is not difficult to understand from the perspective of physics. A higher degree of quantum correlation leads to a higher measurement sensitivity. Additionally, it is worth noting that here we use the actual experimental parameter $\kappa = 10^{-4}$ in the case of cold atomic system [51, 52]. Compared to the vapor atomic system, the interferometer with cold atoms provides the better performance in the QND measurement due to the larger AC-Stark coefficient.

3.2. Effect of losses

There exist inevitable losses in the real experiment, which will bring negative effect on the measurement sensitivity. Here we investigate the effect of losses on the interferometer. The lossy model is shown in figure 4. After taking into account losses, $\hat{S}_2$, $\hat{a}_4$ and $\hat{a}_1$ in terms of the lossless case described in the previous section can be rewritten as

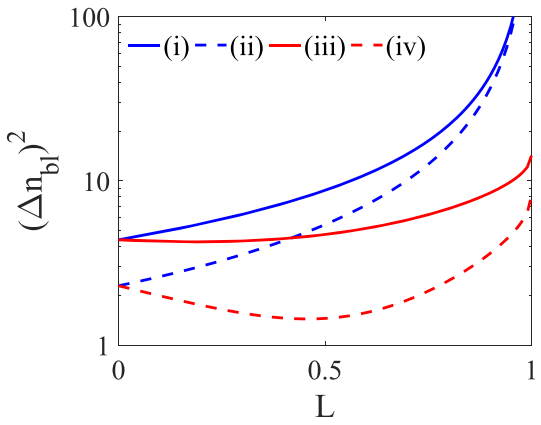

Figure 5. Plot of the optimal sensitivity as a function of the losses for four scenarios: (i) $L_2 = 0$ and $R = 0$, (ii) $L_2 = 0$ and $R = 0.1$, (iii) $L_1 = 0$ and $R = 0$, and (iv) $L_1 = 0$ and $R = 0.1$. In all cases, $\kappa = 10^{-4}$, $g = 1$, $N_a = 10^7$, and $e^{-\Gamma\tau} = 0.9$.

$$\begin{aligned}\hat{S}_{2l} &= \hat{S}_2 e^{-\Gamma\tau} + \hat{F},\\ \hat{a}_{4l} &= \sqrt{1-L_2}\hat{a}_4 + \sqrt{L_2}\hat{v}_2,\\ \hat{a}_{1l} &= \sqrt{1-L_1}\hat{a}_1 + \sqrt{L_1}\hat{v}_1,\end{aligned} \tag{24}$$

where the subscript l represents that the losses are taken into account. L_j $(j = 1, 2)$ denotes the reflectivity of the virtual BS which is used to simulate the photon losses and v_j $(j = 1, 2)$ corresponds to the introduced vacuum noise. $e^{-\Gamma\tau}$ denotes the atomic decoherence losses and $\langle \hat{F}\hat{F}^\dagger \rangle = 1 - e^{-2\Gamma\tau}$ guarantees the consistency of the operator property of $\hat{S}_{2l}$. The input–output relation for the lossy case of $\hat{a}_5$ becomes

$$\begin{aligned}\hat{a}_{5l} = \hat{a}_0 &\frac{G_1 G_2\sqrt{(1-L_1)(1-L_2)}e^{i\phi} + g_1 g_2\sqrt{(1-R)(1-L_1)}e^{-\Gamma\tau}e^{i(\theta_2-\theta_1+\phi-\varphi)} + G_2\sqrt{R(1-L_2)}}{G_1\sqrt{R(1-L_1)}e^{i\phi}+1}\\ + \hat{S}_0^\dagger &\frac{G_2 g_1\sqrt{(1-R)(1-L_2)}e^{i\theta_1} + g_2\sqrt{R(1-L_1)}e^{-\Gamma\tau}e^{i(\theta_2-\varphi+\phi)} + G_1 g_2 e^{-\Gamma\tau}e^{i(\theta_2-\varphi)}}{G_1\sqrt{R(1-L_1)}e^{i\phi}+1}\\ + \hat{v}_1 &\frac{G_1 G_2\sqrt{L_1(1-R)(1-L_2)}e^{i\phi} + g_1 g_2\sqrt{L_1}e^{-\Gamma\tau}e^{i(\theta_2-\theta_1+\phi-\varphi)}}{G_1\sqrt{R(1-L_1)}e^{i\phi}+1} + \hat{v}_2 G_2\sqrt{L_2} + \hat{F}^\dagger g_2 e^{i\theta_2}.\end{aligned} \tag{25}$$

In the case of $L_1 = L_2 = 0$ and $e^{-\Gamma\tau} = 1$ (i.e. no losses), this expression can be simplified and consistent with equation (5). For the balanced case and for $\phi = \pi$, the sensitivity under the lossy condition can be shown to be of the form

$$(\Delta n_{bl})^2 = \frac{\mathcal{H}\mathcal{H}^* + \mathcal{I}\mathcal{I}^* + \mathcal{J}\mathcal{J}^* + G^2 L_2 + g^2\left(1 - e^{-2\Gamma\tau}\right)}{\left[-iN_a^{1/2}\partial\left(\mathcal{H} - \mathcal{H}^*\right)/\partial n_b\right]^2}, \tag{26}$$

with

$$\begin{aligned}\mathcal{H} &= \frac{g^2\sqrt{(1-R)(1-L_1)}e^{-\Gamma\tau}e^{-i\kappa n_b} + G\sqrt{R(1-L_2)} - G^2\sqrt{(1-L_1)(1-L_2)}}{1 - G\sqrt{R(1-L_1)}}\\ \mathcal{I} &= \frac{g\sqrt{R(1-L_1)}e^{-\Gamma\tau}e^{-i\kappa n_b} - Gge^{-\Gamma\tau}e^{-i\kappa n_b} + Gg\sqrt{(1-R)(1-L_2)}}{1 - G\sqrt{R(1-L_1)}}\\ \mathcal{J} &= \frac{g^2\sqrt{L_1}e^{-\Gamma\tau}e^{-i\kappa n_b} - G^2\sqrt{L_1(1-R)(1-L_2)}}{1 - G\sqrt{R(1-L_1)}}.\end{aligned} \tag{27}$$

One can find that the sensitivity under the lossy condition also achieves its minimum when κn_b is 0.

In figure 5 the optimal sensitivity is plotted as a function of the losses for four scenarios: (i) $L_2 = 0$ and $R = 0$, (ii) $L_2 = 0$ and $R = 0.1$, (iii) $L_1 = 0$ and $R = 0$, and (iv) $L_1 = 0$ and $R = 0.1$. It can be seen from these plots that in all cases, the sensitivities degrade with photon losses. Nevertheless, with the increase of photon losses, the sensitivities in the case of (iii) and (iv) decrease more slowly. This indicates that this proposed interferometer is more tolerant with the photon losses L_2 compared to the photon losses L_1 in feedback path. The reason behind the phenomenon is that the photon losses in feedback path affect the quantum

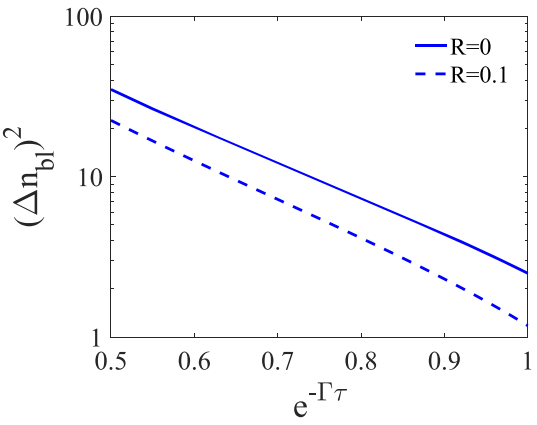

Figure 6. Plot of the optimal sensitivity as a function of the atomic decoherence losses, where $\kappa = 10^{-4}$, $g = 1$, $N_a = 10^7$ and $L_1 = L_2 = 0$.

correlation between the atomic spin wave and optical wave, which is highly fragile and quickly degrades with photon losses. Furthermore, by comparing (i) and (ii), (iii) and (iv), one can find that the feedback control can mitigate the effect of losses on the sensitivity. Additionally, note that in our scheme, the optical field travels out of the atomic ensemble while the atomic spin wave stays in the atomic ensemble. Within the coherence time, the atomic decoherence loss is small, and then we set $e^{-\Gamma\tau} = 0.9$.

Next, the effect of the atomic decoherence losses is analyzed. As shown in figure 6, the blue solid line and the blue dashed line represent the situations with a feedback ratio of $R = 0$ and $R = 0.1$, respectively. We can observe that the sensitivities degrade with the atomic decoherence losses. Additionally, the sensitivity decreases more rapidly under atomic decoherence losses than it does under photon losses. Nevertheless, feedback control can mitigate the effect of losses on the sensitivity.

4. Discussion and conclusion

Experimental consideration of the implementation of the scheme may be performed in a cold rubidium atomic system. The energy levels of the Rb atom are shown in figure 1(b), where state $|e\rangle$ is the excited state $|5^2P_{1/2}, F = 2\rangle$, and states $|g\rangle$ and $|m\rangle$ are the two ground states $|5^2S_{1/2}, F = 1, 2\rangle$ from hyperfine splitting. In the case of cold rubidium atoms, due to the weak Doppler broadening the detuning of the signal field from the transition $|5^2S_{1/2}, F = 2\rangle \rightarrow |5^2P_{1/2}, F = 2\rangle$ can be decreased to 120 MHz. The interaction between the signal field and atoms will induce an atomic phase shift that is proportional to the photon number of the signal field. With a detuning 120 MHz, the AC-Stark coupling coefficient κ is $\sim 10^{-4}$ rad per photon. This is feasible in the experiment [51, 52]. In addition, experimental implementations of coherent feedback strategies have demonstrated significant efficacy in facilitating various tasks, such as stabilization of entanglement [53], swaps of quantum states [32], sympathetic cooling [54] and qubit control [55]. This indicates that the current experimental technology for coherent feedback is very mature, which lays a solid foundation for the experimental implementation of our scheme. Furthermore, it is worth noting the difference between coherent feedback and measurement-based feedback [56, 57]. In contrast to measurement-based feedback, coherent feedback operates independently of measurement process, thereby avoiding issues such as decoherence, dispersion, latency, and other imperfections in data processing and optical control.

Our scheme has some advantages compared to other schemes. First, the atom-light hybrid interferometer system utilizes the stimulated Raman scattering process in the atomic system, which enables the phase of the Stokes optical field and the atomic spin wave to be mutually correlated [58]. This ensures the stability of the phase. Such phase stability is crucial for interferometric measurements, as it can effectively reduce measurement errors caused by phase fluctuations. Second, this type of interferometer is sensitive to both optical and atomic phase shift, thus it can be applied to a variety of measurement scenarios. The third merit lies in its robust performance against losses.

In conclusion, we have theoretically proposed a FALCI and applied it to the QND measurement of photon number by means of the AC-Stark effect. The FALCI performs the measurement by harnessing the interference between the quantum-correlated atoms and light, in which a BS with adjustable reflectivity is employed as a feedback controller to further manipulate it. We find that the quantum correlation can be enhanced by tuning the feedback ratio, and the optimal feedback ratio is given. Furthermore, it is found that

a suitable feedback ratio can also enhance the QND measurement sensitivity. In addition, the FALCI is robust to the losses. The effect of losses on the sensitivity can be mitigated through the feedback control. Our results lay a solid foundation for the practical application of the FALCI in quantum enhanced metrology.

Data availability statement

All data that support the findings of this study are included within the article (and any supplementary files).

Acknowledgments

This work is supported by the National Natural Science Foundation of China(12404418); Fundamental Research Program of Shanxi Province(202303021212171).

References

[1] Braginsky V B, Vorontsov Y I and Thorne K S 1980 Quantum nondemolition measurements *Science* **209** 547
[2] Grangier P, Levenson J A and Poizat J 1998 Quantum non-demolition measurements in optics *Nature* **396** 537
[3] Caves C M, Thorne K S, Drever R W P, Sandberg V D and Zimmermann M 1980 On the measurement of a weak classical force coupled to a quantum-mechanical oscillator. I. Issues of principle *Rev. Mod. Phys.* **52** 341
[4] Braginsky V B and Khalili F Y 1996 Quantum nondemolition measurements: the route from toys to tools *Rev. Mod. Phys.* **68** 1
[5] Bocko M F and Onofrio R 1996 On the measurement of a weak classical force coupled to a harmonic oscillator: experimental progress *Rev. Mod. Phys.* **68** 755
[6] Scully M O and Zubairy M S 1997 *Quantum Optics* (Cambridge University Press)
[7] Walls D F and Milburn G J 2008 *Quantum Optics* 2nd edn (Springer)
[8] Bao H *et al* 2020 Spin squeezing of 10^{11} atoms by prediction and retrodiction measurements *Nature* **581** 159
[9] Eberle T, Steinlechner S, Bauchrowitz J, Händchen V, Vahlbruch H, Mehmet M, Müller-Ebhardt H and Schnabel R 2010 Quantum enhancement of the zero-area sagnac interferometer topology for gravitational wave detection *Phys. Rev. Lett.* **104** 251102
[10] Pitkin M, Reid S, Rowan S and Hough J 2011 Gravitational wave detection by interferometry (ground and space) *Living Rev. Relativ.* **14** 5
[11] Kong L-D, Zhang T-Z, Liu X-Y, Li H, Wang Z, Xie X-M and You L-X 2024 Large-inductance superconducting microstrip photon detector enabling 10 photon number resolution *Adv. Photon.* **6** 016004
[12] Hadfield R H 2009 Single-photon detectors for optical quantum information applications *Nat. Photon.* **3** 696
[13] Imoto N, Haus H A and Yamamoto Y 1985 Quantum nondemolition measurement of the photon number via the optical Kerr effect *Phys. Rev. A* **32** 2287
[14] Holland M J, Walls D F and Zoller P 1991 Quantum nondemolition measurements of photon number by atomic beam deflection *Phys. Rev. Lett.* **67** 1716
[15] Friberg S R, Machida S and Yamamoto Y 1992 Quantum-nondemolition measurement of the photon number of an optical soliton *Phys. Rev. Lett.* **69** 3165
[16] Jacobs K, Tombesi P, Collett M J and Walls D F 1994 Quantum-nondemolition measurement of photon number using radiation pressure *Phys. Rev. A* **49** 1961
[17] Sakai Y, Hawkins R J and Friberg S R 1990 Soliton-collision interferometer for the quantum nondemolition measurement of photon number: numerical results *Opt. Lett.* **15** 239
[18] Kok P, Lee H and Dowling J P 2002 Single-photon quantum-nondemolition detectors constructed with linear optics and projective measurements *Phys. Rev. A* **66** 063814
[19] Gerry C C and Bui T 2008 Quantum non-demolition measurement of photon number using weak nonlinearities *Phys. Lett. A* **372** 7101
[20] Munro W J, Nemoto K, Beausoleil R G and Spiller T P 2005 High-efficiency quantum-nondemolition single-photonnumber-resolving detector *Phys. Rev. A* **71** 033819
[21] Nogues G, Rauschenbeutel A, Osnaghi S, Brune M, Raimond J M and Haroche S 1999 Seeing a single photon without destroying it *Nature* **400** 239
[22] Xiao Y F, Ozdemir S K, Gaddam V, Dong C H, Imoto N and Yang L 2008 Quantum nondemolition measurement of photon number via optical Kerr effect in an ultra-high-Q microtoroid cavity *Opt. Express* **16** 21462
[23] Ludwig M, Safavi-Naeini A H, Painter O and Marquardt F 2012 Enhanced quantum nonlinearities in a two-mode optomechanical system *Phys. Rev. Lett.* **109** 063601
[24] Malz D and Cirac J I 2020 Nondestructive photon counting in waveguide QED *Phys. Rev. Res.* **2** 033091
[25] Liu J, Chen H T and Segal D 2020 Quantum nondemolition photon counting with a hybrid electromechanical probe *Phys. Rev. A* **102** 061501(R)
[26] Balybin S N, Matsko A B, Khalili F Y, Strekalov D V, Ilchenko V S, Savchenkov A A, Lebedev N M and Bilenko I A 2022 Quantum nondemolition measurements of photon number in monolithic microcavities *Phys. Rev. A* **106** 013720
[27] Balybin S, Salykina D and Khalili F Y 2023 Improving the sensitivity of Kerr quantum nondemolition measurement via squeezed light *Phys. Rev. A* **108** 053708
[28] Chen S Y, Chen L Q, Ou Z Y and Zhang W 2017 Quantum non-demolition measurement of photon number with atom-light interferometers *Opt. Express* **25** 31827
[29] Fan D H, Chen S Y, Yu Z F, Zhang K and Chen L Q 2020 Quality estimation of non-demolition measurement with lossy atom-light hybrid interferometers *Opt. Express* **28** 9875
[30] Jiao G-F, Zhang K, Chen L Q, Yuan C-H and Zhang W 2022 Quantum non-demolition measurement based on an SU(1,1)-SU(2)-concatenated atom-light hybrid interferometer *Photon. Res.* **10** 475
[31] Wiseman H M and Milburn G J 1994 All-optical versus electro-optical quantum-limited feedback *Phys. Rev. A* **49** 4110

[32] Nelson R J, Weinstein Y, Cory D and Lloyd S 2000 Experimental demonstration of fully coherent quantum feedback *Phys. Rev. Lett.* **85** 3045
[33] Lloyd S 2000 Coherent quantum feedback *Phys. Rev. A* **62** 022108
[34] Pan X, Chen H, Wei T, Zhang J, Marino A M, Treps N, Glasser R T and Jing J 2018 Experimental realization of a feedback optical parametric amplifier with four-wave mixing *Phys. Rev. B* **97** 161115(R)
[35] Zhong Y and Jing J 2020 Enhancement of tripartite quantum correlation by coherent feedback control *Phys. Rev. A* **101** 023813
[36] Xin J, Pan X, Lu X-M, Kong J, Li G and Li X 2020 Entanglement enhancement from a two-port feedback optical parametric amplifier *Phys. Rev. Appl.* **14** 024015
[37] Pan X, Wei T, Zhang K and Jing J 2024 Experimental realization of active nonlinear feedback control from hot rubidium vapor *Quantum Sci. Technol.* **9** 045020
[38] He H, Zhang K and Jing J 2024 Hexapartite coherent feedback control in four-wave mixing with a spatially structured pump *Phys. Rev. A* **109** 062409
[39] Liao D, Xin J and Jing J 2021 Nonlinear interferometer based on two-port feedback nondegenerate optical parametric amplification *Opt. Commun.* **496** 127137
[40] Liang X, Zhao J, Yan Y, Huang W, Yuan C-H and Chen L Q 2024 Coherent feedback enhanced quantum-dense metrology in a lossy environment *Opt. Express* **32** 12982
[41] Jiao G-F 2024 Enhanced phase sensitivity in a feedback-assisted interferometer *New J. Phys.* **26** 083005
[42] Jiao G-F 2024 Enhancing phase sensitivity by a nonlinear-feedback-assisted interferometer *Opt. Express* **32** 46150
[43] Yamamoto N 2016 Quantum feedback amplification *Phys. Rev. Appl.* **5** 044012
[44] Bemani F, Černotík O, Manetta A, Hoff U B, Andersen U L and Filip R 2024 Optical and mechanical squeezing with coherent feedback control beyond the resolved-sideband regime *Phys. Rev. Appl.* **22** 044028
[45] Ou Z Y 2008 Efficient conversion between photons and between photon and atom by stimulated emission *Phys. Rev. A* **78** 023819
[46] Chen B, Qiu C, Chen S, Guo J, Chen L Q, Ou Z Y and Zhang W 2015 Atom-light hybrid interferometer *Phys. Rev. Lett.* **115** 043602
[47] Jasperse M, Turner L D and Scholten R E 2011 Relative intensity squeezing by four-wave mixing with loss: an analytic model and experimental diagnostic *Opt. Express* **19** 3765
[48] Autler S H and Townes C H 1955 Stark effect in rapidly varying fields *Phys. Rev.* **100** 703
[49] Hammerer K, Sørensen A S and Polzik E S 2010 Quantum interface between light and atomic ensembles *Rev. Mod. Phys.* **82** 1041
[50] Heitler W 1954 *The Quantum Theory of Radiation* (Oxford University)
[51] Du S, Oh E, Wen J and Rubin M H 2007 Four-wave mixing in three-level systems: interference and entanglement *Phys. Rev. A* **76** 013803
[52] Kruse D, Ruder M, Benhelm J, Cube C V, Zimmermann C, Courteille P W, Elsasser T, Nagorny B and Hemmerich A 2003 Cold atoms in a high-Q ring cavity *Phys. Rev. A* **67** 051802
[53] Shankar S, Hatridge M, Leghtas Z, Sliwa K, Narla A, Vool U, Girvin S M, Frunzio L, Mirrahimi M and Devoret M H 2013 Autonomously stabilized entanglement between two superconducting quantum bits *Nature* **504** 419
[54] Schmid G-L, Ngai C T, Ernzer M, Aguilera M B, Karg T M and Treutlein P 2022 Coherent feedback cooling of a nanomechanical membrane with atomic spins *Phys. Rev. X* **12** 011020
[55] Hirose M and Cappellaro P 2016 Coherent feedback control of a single qubit in diamond *Nature* **532** 77
[56] Meng C and Bowen W P 2024 Enhancement of mechanical squeezing via feedback control (arXiv:2402.17460)
[57] Kroeger K, Dogra N, Rosa-Medina R, Paluch M, Ferri F, Donner T and Esslinger T 2020 Continuous feedback on a quantum gas coupled to an optical cavity *New J. Phys.* **22** 033020
[58] Bian C-L, Chen L-Q, Zhang G-W, Ou Z Y and Zhang W 2012 Retrieval of phase memory in two independent atomic ensembles by Raman process *Europhys. Lett.* **97** 34005